Int. J. Heat Mass Transfer. Vol. 34, No. 3, pp. 703–709, 1991
Printed in Great Britain

0017–9310/91 $3.00 + 0.00
Pergamon Press plc

Natural convection in a Hele–Shaw cell

S. S. VORONTSOV, A. V. GORIN, V. Ye. NAKORYAKOV,
A. G. KHORUZHENKO and V. M. CHUPIN

Institute of Thermophysics, Siberian Branch of the USSR Academy of Sciences, Novosibirsk, 630090, U.S.S.R.

(*Received* 26 *May* 1990)

Abstract—Theoretical and experimental analysis of natural convection heat transfer in the Hele–Shaw cell on narrow side walls is presented. Cases of constant wall temperature and uniform wall heat flux are studied. Temperature profiles in a thermal boundary layer on a heated side wall are measured by a scanning thermocouple. Thermograms of flow in the cell are obtained by means of an optomechanical IR imaging system. The results of theoretical and experimental studies are in good agreement. The theoretical model of natural convection heat transfer in a Hele–Shaw cell is shown to be in complete accordance with the model of natural convection heat transfer in a porous medium, with the complex $h^2/12$ playing the role of permeability in the cell.

1. INTRODUCTION

THE FLOW of a viscous fluid in a narrow slot between parallel plates (the Hele–Shaw cell) is often resorted to by researchers for modelling fluid filtration through a porous medium [1]. This analogy is based on the similarity between the differential filtration equations and those for a viscous fluid motion between parallel plates. The principles of the Hele–Shaw flow theory are briefly outlined by Lamb [2]. As a model object for investigating heat transfer processes in a porous medium this device was used only in work [3] to analyse the rise of a plume from a horizontal line heat source in a porous medium; the author presents his experimental data on the change in the plume front velocity in a narrow slot. The experiments were made with a weak solution of potassium permanganate injected through a capillary.

Apart from being the model object for studying flow in a porous medium, the Hele–Shaw cell is also used for studying heat transfer in a narrow slot between plates with the aim to aid in the understanding and optimization of heat transfer processes in cooled thermally stressed elements of radioelectronic equipment, in the calculation and construction of modern heat exchangers, etc.

This paper presents the results of theoretical and experimental investigations of the problem of natural convection heat transfer on a vertical narrow side wall of a Hele–Shaw cell.

2. STATEMENT OF THE PROBLEM

Consider natural convection adjacent to a narrow vertical side wall of a Hele–Shaw cell formed by thermally insulated vertical plates. In the mathematical formulation of the problem it is assumed that (i) the properties of the fluid such as viscosity, thermal conductivity, specific heats and thermal expansion coefficient are constant and (ii) the Boussinesq approximation $\rho = \rho_\infty(1-\beta(T-T_\infty))$ can be applied. Under these assumptions, the governing equations are given by

$$\nabla\cdot\mathbf{v} = 0$$
$$(\mathbf{v}\cdot\nabla)\mathbf{v} = -\nabla p+\rho_\infty g\beta(T-T_\infty)\nabla x+\mu\Delta\mathbf{v}$$
$$(\mathbf{v}\cdot\nabla)T = a\Delta T \qquad (1)$$

where $\mathbf{v}$, p and T are the velocity, pressure and temperature of fluid; the subscript ∞ denotes the fluid parameters outside the boundary layer on the plate; $\Delta = \partial^2/\partial x^2+\partial^2/\partial y^2+\partial^2/\partial z^2$ is the Laplace operator; $\Delta = (\partial/\partial x)\mathbf{i}+(\partial/\partial y)\mathbf{j}+(\partial/\partial z)\mathbf{k}$. The directions of the axes of the Cartesian coordinate system are shown in Fig. 1, the values $z = \pm h/2$ correspond to the positions of boundaries. It is assumed that there is no motion anywhere in the direction of the z-axis in the cell (the velocity component $w = 0$) and that the Poiseuille profile is realized for the longitudinal and transverse velocity components

$$u = \tfrac{3}{2}u_0(x,y)[1-4z^2/h^2]$$
$$v = \tfrac{3}{2}v_0(x,y)[1-4z^2/h^2]. \qquad (2)$$

The fluid temperature is assumed to be constant in the direction of z, i.e.

$$T = T(x,y). \qquad (3)$$

Integration of system (1), taking relations (2) and (3) into account, over the slot cross-section (from $-h/2$ to $h/2$) in the boundary layer approximation yields

$$\partial u_0/\partial x+\partial v_0/\partial y = 0$$
$$\tfrac{6}{5}(u_0\partial u_0/\partial x+v_0\partial u_0/\partial y) = \nu\partial^2 u_0/\partial y^2 - 12\nu u_0/h^2+g\beta(T-T_\infty)$$
$$u_0\partial T/\partial x+v_0\partial T/\partial y = a\partial^2 T/\partial y^2. \qquad (4)$$

NOMENCLATURE

A constant in equation (6) [°C m^{-1}]
a thermal diffusivity of fluid [m^2 s^{-1}]
f dimensionless stream function
g gravity acceleration [m s^{-2}]
H height of cell
h thickness of cell [m]
L length of cell [m]
Nu_x local Nusselt number
q heat flux [W m^{-2}]
Ra local Rayleigh number in the case of constant wall temperature, $g\beta(T_w - T_\infty)h^2x/(12va)$
Ra_* local Rayleigh number in the case of uniform wall heat flux, $g\beta q_w h^2x^2/(12va\lambda)$
u, v, w velocity vector projection onto axes x, y, z, respectively [m s^{-1}]
P electric power of a heater [W]
x, y, z axes of Cartesian coordinate system [m].

Greek symbols
α heat transfer coefficient [W m^{-2} s^{-1}]
β coefficient of thermal expansion [K^{-1}]
γ constant defined in equation (6)
η dimensionless self-similar independent coordinate, $Ra^{1/2}\,y/x$ or $Ra_*^{1/3}\,y/x$
θ dimensionless temperature, $(T-T_\infty)/(T_w-T_\infty)$ or $(T-T_\infty)Ra_*^{1/3}/(q_w x)$
λ thermal conductivity of fluid [W m^{-1} K^{-1}]
μ viscosity of fluid [kg m^{-1} s^{-1}]
ν kinematic viscosity of fluid [m^2 s^{-1}]
ρ density of fluid [kg m^{-3}]
ψ stream function [m^2 s^{-1}].

Superscript
$'$ differentiation with respect to η.

Subscripts
w condition at the wall
0 quantities independent of z.

Without viscous and inertia terms the second equation of system (4) takes on the form

$$\partial u_0/\partial x + \partial v_0/\partial y = 0$$
$$u_0 = g\beta(T-T_\infty)h^2/(12\nu)$$
$$u_0\partial T/\partial x + v_0\partial T/\partial y = a\partial^2 T/\partial y^2. \quad (5)$$

2.1. *Constant wall temperature*

In the general case, when the plate temperature T_w is the power function of the longitudinal coordinate x, the boundary conditions are

$$T = T_w = T_\infty + Ax^\gamma, \quad v_0 = 0 \quad \text{at } y = 0 \quad (6)$$
$$T = T_\infty, \quad u_0 = 0 \quad \text{for } y \to \infty. \quad (7)$$

To seek the similarity solutions for equations (5)–(7), introduce the dimensionless self-similar variables as follows:

$$\eta = Ra^{1/2}\,y/x, \quad \psi = a\,Ra^{1/2} f(\eta),$$
$$\theta = (T-T_\infty)/(T_w-T_\infty) \quad (8)$$

where

$$Ra = g\beta(T-T_\infty)h^2x/(12va)$$

whereas ψ is the stream function such that

$$u_0 = \partial\psi/\partial y, \quad v_0 = -\partial\psi/\partial x. \quad (9)$$

The governing equations (5) with boundary conditions (6) and (7) in terms of these variables are

$$f' = \theta$$
$$\theta'' + \frac{\gamma+1}{2} f\theta' - \gamma f'\theta = 0$$
$$\theta = 1, \quad f = 0 \quad \text{at} \quad \eta = 0$$
$$\theta = 0, \quad f' = 0 \quad \text{for} \quad \eta \to \infty. \quad (10)$$

System (10) fully coincides with the governing equations for free convection adjacent to a vertical plate in a saturated porous medium [4], consequently, the dimensionless heat transfer law [4] is valid for our problem

$$Nu_x = -\theta'(0)Ra^{1/2} \quad (11)$$

where $Nu_x = \alpha x/\lambda$. The only difference lies in the form of Rayleigh number representation (in the case of a porous medium $Ra = g\beta(T-T_\infty)Kx/(\nu a)$, where K is the permeability of a porous medium). In the general case, $\theta'(0)$ is a function of the parameter γ; for an isothermal plate $-\theta'(0) = 0.444$.

The analogy obtained confirms the validity of modelling free-convective heat transfer in a porous medium by natural convection in Hele–Shaw natural convective flows.

2.2. *Uniform wall heat flux*

In this case conditions (6) should be replaced by

$$\partial T/\partial y = -q_w/\lambda, \quad v_0 = 0 \quad \text{at} \quad y = 0 \quad (12)$$

and the self-similar variables should be written as

$$\eta = Ra_*^{1/3}\,y/x, \quad \psi = a\,Ra_*^{1/3} f(\eta),$$

$$\theta = (T - T_\infty)\lambda\, Ra_*^{1/3}/(q_w x)$$

where

$$Ra_* = g\beta q_w h^2 x^2/(12va\lambda).$$

Now the heat transfer problem is formulated as

$$f' = \theta$$

$$\theta'' + \tfrac{2}{3} f\theta' - \tfrac{1}{3} f'\theta = 0$$

$$\theta' = -1, \quad f = 0 \quad \text{at} \quad \eta = 0$$

$$\theta = 0, \quad f' = 0 \quad \text{for} \quad \eta \to \infty. \qquad (13)$$

The local Nusselt number was found to be

$$Nu_x = [\theta(0)^{-1}]Ra_*^{1/3}. \qquad (14)$$

The numerical solution of the system of equations (13) gives the value $[\theta(0)]^{-1} = 0.772$.

3. EXPERIMENTAL APPARATUS AND THE TECHNIQUE OF MEASUREMENTS

The study of heat transfer in a Hele–Shaw cell was carried out on two rigs that differ by boundary conditions on narrow side walls. Figure 1 shows the schematic diagram of the rig for the case of the boundary condition $q_w = \text{const}$.

Heater 1 and the rectangular copper tube 2 of 9×5 mm^2 cross-section for pumping cold water are clamped between two 26 mm thick lucite plates with the use of gaskets.

The dimensions of the working cavity are: $H = 0.22$ m, $L = 0.19$ m; $h = 2 \times 10^{-3}$ m. The heater is made of nichrome foil of thickness 10^{-4} m, width 1.9×10^{-3} m and length 0.21 m, and is pasted onto the end face of a foam plastic plate.

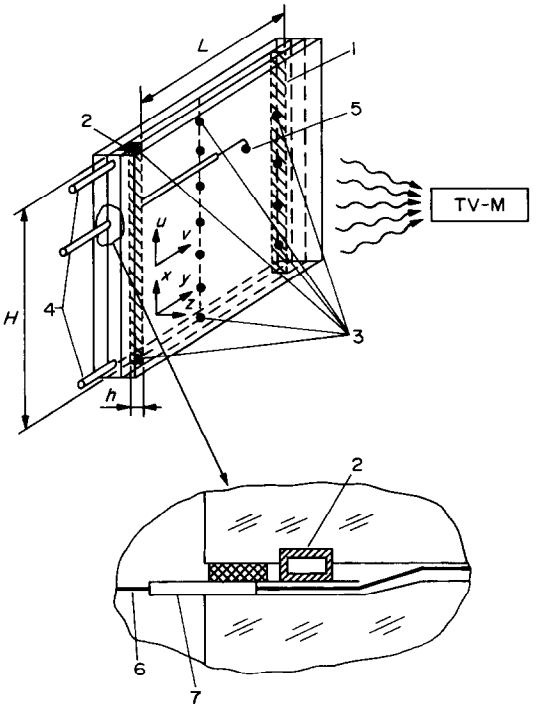

FIG. 1. Schematic diagram of the set-up.

Through the holes in this plate, five nichrome–constantan thermocouples three of diameter 10^{-4} m were introduced at a distance of 0.05 m from one another and were contact-welded to the heater to measure its temperature.

The heater was used as a working plate for studying heat transfer. The heating was realized by direct current from a controlled power source. The electric power supplied was determined from the readings of an ammeter and digital voltmeter.

The opposite side wall of the cell was cooled by water of temperature T_0 pumped by a thermostat through the rectangular copper tube and pipe connections 4. The tube temperature was measured at the lower and upper points. The change in the temperature of the cooling wall amounted to no more than 5% of the temperature difference $(T_w - T_0)$, thus allowing it to be considered isothermal.

The cavity bottom was hermetically sealed with a rubber gasket, whereas the top was open. In some of the runs, the top was closed. The working fluid was degassed water.

In the rig with isothermal side walls, the heating and cooling were realized by pumping water of fixed temperature by two thermostats through 9×5 mm^2 rectangular copper channels.

The copper channels for cold and hot water were embedded in milled grooves of depth 7×10^{-3} m and width 5×10^{-3} m in the lucite wall (for the case of $q_w = \text{const}$.), in the foam plastic wall (in the case when $T_w = \text{const}$.). The temperatures of the cooling and heating walls were measured by thermocouples at two points.

The temperature profiles in the thermal boundary layer on the heated side wall were measured by scanning microthermocouple 5 introduced from the cooling wall side at four levels along the height: 0.025, 0.046, 0.064, 0.147 m. Also shown in this figure are the layout of the channel for pumping water and the scheme of insertion of the scanning microthermocouple. The scanning thermocouple made of nichrome–constantan wire 6×10^{-5} m in diameter was placed in a bent stainless steel pipe jacket with an external diameter of 8×10^{-4} m. The end of the thermocouple extended 0.012 m beyond the jacket. The side of the thermocouple insertion was sealed with a water-resistant adhesive. The jacket was confined within directing pipe 7 with the external diameter of 2×10^{-3} m located in the conical recess in the side lucite wall. The microthermocouple moved in the plane perpendicular to the heater. The motion was controlled by a pointer indicator accurate within 10^{-5} m.

The water temperature in the cell was measured on the vertical symmetry axis by seven nichrome–constantan thermocouples 3 that were inserted

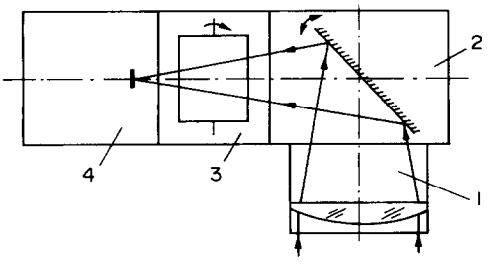

FIG. 2. Optomechanical scheme of the TV-M system: 1, modulus of the lens; 2, modulus of the frame scanning; 3, modulus of the line scanning; 4, modulus of radiation receiver.

through the holes along the central line of the lucite wall. The distance between the thermocouples was 0.04 m in the set-up with q_w = const. and 0.05 m in the set-up with T_w = const., with the lower thermocouple being located on the cavity bottom.

Visualization of the temperature field of the working cavity was carried out with the use of an optomechanical infra-red imaging system TV-M [5].

The system consists of an optomechanical part and an analogue-digital electronic block and operates as follows. By means of a germanium lens, the image of the object is created in the infra-red spectrum region. The image is scanned by the optomechanical system relative to the quasi-point site of a radiation detector cooled by liquid nitrogen. The rate of scanning is 1 frame s^{-1}. The scheme of the optomechanical part is presented in Fig. 2. Video signal, sync-pulses (SP) of frames and lines are fed to the analogue-digital electronic block. The functional scheme of the device is given in Fig. 3. The electronic block includes a power source and blocks that control the recording and processing of data. The basis parameters of the system are:

spectral range	2.5–5.5 μm
space resolution	100×100 elements
scanning angle	$12^\circ \times 12^\circ$
word length of digital transformation	8 bites
rate of scanning	1 frame s^{-1}
temperature resolution obtained with the use of the black body model without accumulation	0.3 °C on the level of 30 °C.

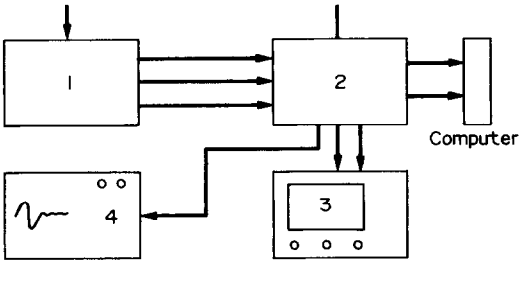

FIG. 3. Functional scheme of the TV-M system: 1, optomechanical part; 2, electronic block; 3, colour display; 4, oscillograph.

The amplitude of the video signal is converted into a digital code and is loaded as buffer memory, with the loading being controlled by the SP from the optomechanical block. Simultaneously, the information from the digital buffer is followed on the colour TV screen in the form of a topogram with a standard television speed. Thus, the scale-time transformation of information is realized.

The electronic part of the system allows one to accumulate information in real time (averaging of the frames being entered), to record the information introduced, and to use different means for representing thermograms. The temperature resolution—the temperature drop corresponding to the transition between the neighbouring colours of the thermogram picture at a satisfactory signal–noise ratio—attained 0.1 °C at the level of 30 °C and above in the course of acquisition of information. It is possible to represent thermograms with multiple use of colour and grayness scales, or in the form of a system of oscillograms. Thermograms taken from the monitor screen are given below.

To obtain thermograms, the lucite side wall was replaced by a stainless steel plate 8×10^{-4} m in thickness. The TV-M system registered the distribution of radiation intensity on that plate. In order to equalize and increase the emissivity coefficient, the wall surface was covered with special paint.

The spreading of temperature along the plate was controlled by thermocouples stamped into it at a distance of 5×10^{-3} m from one another. It appeared to be insignificant, and one could observe the temperature gradient accurate to within 0.1 K per isotherm.

The errors of temperature measurement by thermocouples in the boundary layer were of the order of ± 0.1°C. Note that the finite dimension of the thermocouple bead (in the present case its dimension is of the order of 1.2×10^{-4} m) leads to the deterioration of spatial resolution. Temperature profiles in the boundary layer shift from the wall, because the thermocouple bead cannot be located on the heater surface. Accordingly, the dimensionless temperature profiles in the boundary layer are displaced by about the bead dimension and the maximum value of θ measured is smaller than unity.

The readings of the microthermocouples were introduced into a computer through a digital voltmeter and were interpreted in the form of the function $Nu_x(Ra)$. The local heat transfer coefficient was calculated by the formula

$$\alpha_x = q/(T_w - T_x) = P/(F(T_w - T_{0x}))$$

where F is the heater area, T_{0x} the water temperature in the core of the cell on the level x reckoned from the

cell bottom. The physical parameters of water were determined at $T_{av} = (T_w = T_{0x})/2$.

The local wall heat flux for the isothermal plate was calculated by the least square method from the measured temperature profile in the thermal boundary layer ($y = 0.1$, 0.2, 0.3, 0.4 and 0.5 mm) at four heights: $x = 0.025$, 0.046, 0.064 and 0.147 m.

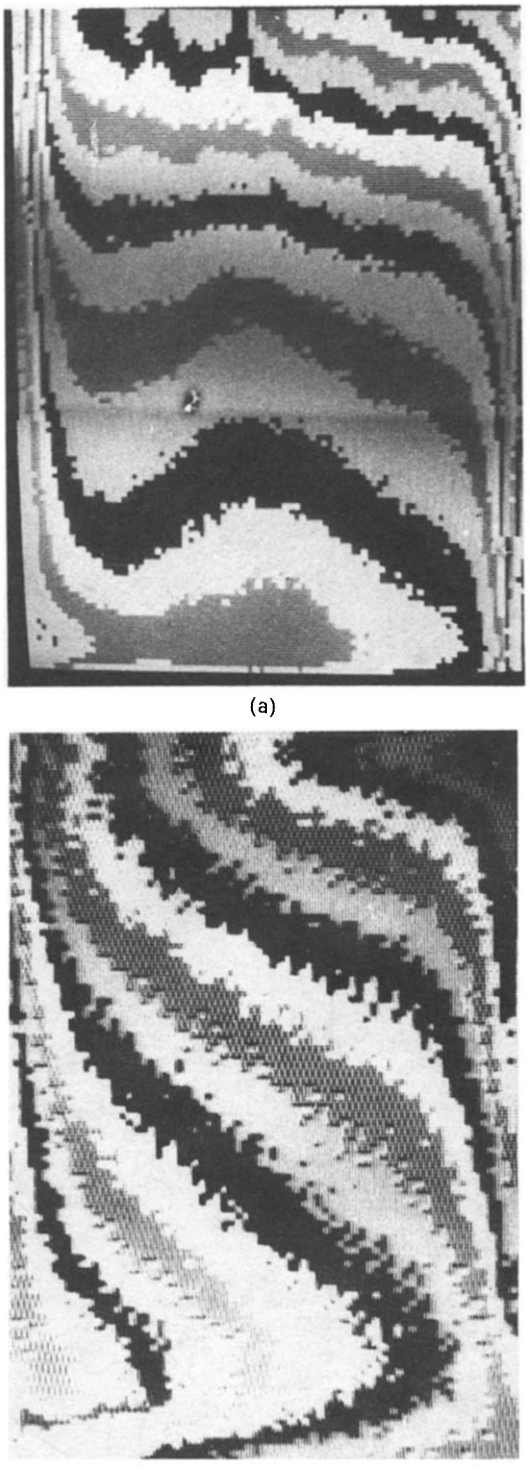

(a)

(b)

FIG. 4. Thermograms of free-convective flow in the Hele–Shaw cell: (a) boundary conditions of the first kind, $T_w = 30$°C, $T_0 = 17$°C; (b) boundary conditions of the second kind $q_w = 1.29 \times 10^5$ W m^{-2}, $T_0 = 17$°C.

Visualization of flow in the Hele–Shaw cell was carried out by injecting violet ink into the upper part of the working cavity. The filming was carried out in reflected light after a time lapse of 20 min.

In the present experiments the temperature of the cooled side wall was specified in the range 10–19°C. In the case of the isothermal boundaries, the temperature of the heated plate varied within the range $T_w = 25$–50°C, whereas for the uniform wall heat flux conditions the working range for the heat flux was $q_w = 6.7 \times 10^3$–1.75×10^5 W m^{-2}. All the experiments given in the present work were carried out for $2/3 \leqslant H_x/L \leqslant 1$; here H_x is the level of the liquid poured into the working cavity.

4. RESULTS AND DISCUSSION

The photographs of isotherms taken from the colour monitor are presented in Fig. 4 for both cases of the boundary conditions. For isothermal walls the regime with $T_0 = 17.2$°C and $T_w = 30$°C is presented and for the isothermal wall heat flux conditions—the regime with $T_0 = 17.2$°C and $q_w = 1.29 \times 10^5$ W m^{-2}. The thermograms reveal the presence of a sharp temperature gradient near the wall and also the stratification of the liquid core.

While the temperature difference $(T_w - T_0)$ increases, the isotherms inside the liquid core tend to a horizontal position.

Figure 5(b) presents the visualization of flow in the Hele–Shaw cell for the case of $q_w = \text{const.}$ and for isothermal walls (Fig. 5(a)). In the present experiments a single-cellular flow was always observed. As the difference $(T_w - T_0)$ increased, the centre of rotation in the case of $q_w = \text{const}$, displaced upwards due to the asymmetry of boundary conditions, and approached the heater. With the decrease in the temperature difference down to 3–4°C, a symmetric flow was developed.

The solution of problem (10) is given in ref. [4]. Non-linear boundary problem (13) was transformed to the sequence of linear Cauchy problems by the methods of quasi-linearization and superposition and was solved numerically by the fourth-order Runge–Kutta–Merson method with automatic selection of the step. A comparison of calculations with the experimental data of the present author given in Fig. 6 in the form of relations for the local Nusselt number (11) (curve 1) and (14) (curve 2). A satisfactory agreement of theory and experiment should be noted, which confirms the validity of the assumption adopted in the mathematical model of the process.

The measured temperature profiles in the boundary layer on the isothermal side cell wall are compared with calculations in Fig. 7. For some heat transfer regimes the deviation from the self-similar profile is observed. Possibly, some uncertainty in the readings of thermocouples is introduced with the disturbances

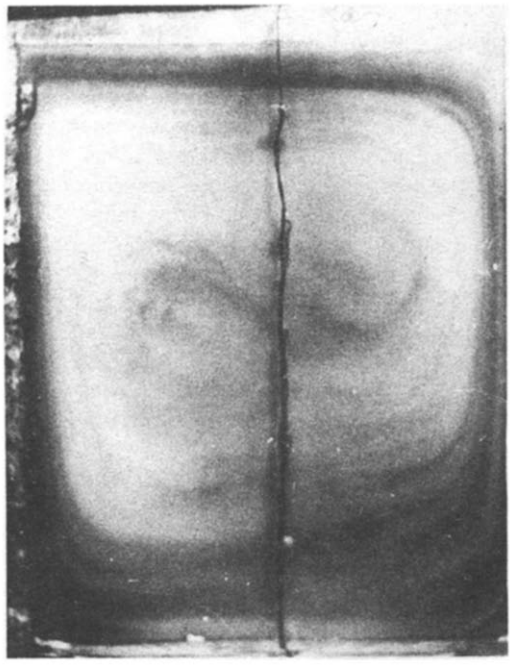

(a)

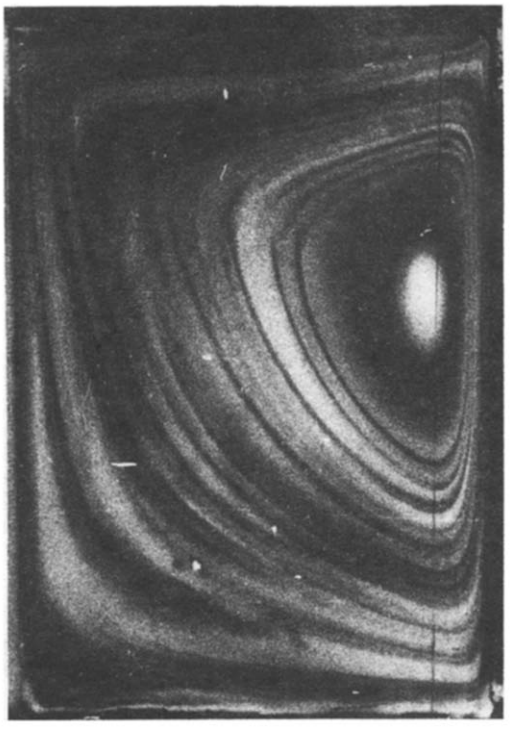

(b)

FIG. 5. Streamlines: (a) boundary conditions of the first kind, $T_w = 30°C$, $T_0 = 17°C$; (b) boundary conditions of the second kind, $q_w = 1.29 \times 10^5$ W m^{-2}.

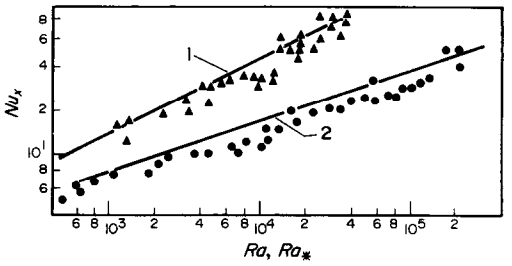

FIG. 6. Local heat transfer coefficient: curve 1, calculation by equation (11), T_w = const.; curve 2, calculation by equation (14), q_w = const.; ▲, ●, experimental data of the authors.

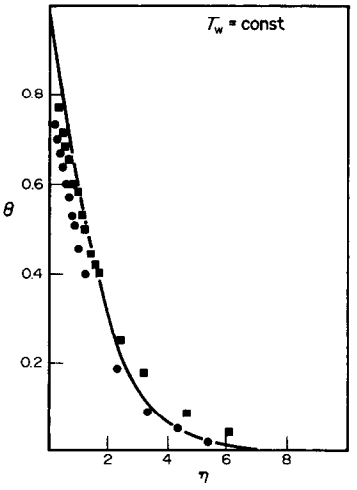

FIG. 7. Temperature profiles in the boundary layer on the vertical plate in the Hele–Shaw cell (boundary conditions with T_w = const.).

induced in the flow by the scanning thermocouples. But in general, the coincidence of theory and experiment should be regarded as satisfactory.

REFERENCES

1. J. Bear, D. Zaslavsky and S. Irmay, *Physical Principles of Water Percolation and Seepage*. UNESCO (1968).
2. H. Lamb, *Hydrodynamics*, 5th Edn. Cambridge University Press, London (1924).
3. R. A. Wooding, Convection in a saturated porous medium at large Rayleigh number and Peclet number, *J. Fluid Mech.* **15**, 527–544 (1962).
4. P. Cheng and W. J. Minkowycz, Free convection about a vertical flat plate embedded in a porous medium with application to heat transfer from a dike, *J. Geophys. Res.* **82**, 2040–2044 (1977).
5. V. V. Bashurov, L. N. Boychuk, S. S. Vorontsov and Yu. N. Vyshenko, Module measuring-computing IR imaging system TV-M. In *Thermovisic Application and Specific Features of the Construction of Thermovision Systems*, pp. 90–97. Sbornik Nauch. Trudov, Moscow (1986).

CONVECTION NATURELLE DANS UNE CELLULE HELE–SHAW

Résumé—On présente une analyse théorique et expérimentale de la convection thermique naturelle dans une cellule Hele–Shaw. On étudie des cas à température pariétale uniforme et à flux thermique uniforme. Les profils de température dans une couche limite thermique sur une paroi chauffée sont mesurés par un thermocouple. Des thermogrammes d'écoulement dans la cellule sont obtenus au moyen d'un système IR optomécanique. Les résultats des études théorique et expérimentale sont en bon accord. Le modèle de la convection naturelle thermique dans une cellule Hele–Shaw est en accord complet avec le modèle de la convection thermique naturelle dans un milieu poreux avec le complexe $h^2/12$ jouant le rôle de la perméabilité dans la cellule.

NATÜRLICHE KONVEKTION IN EINER HELE/SHAW-ZELLE

Zusammenfassung—Der Wärmeübergang durch natürliche Konvektion zwischen den dicht beieinanderstehenden Seitenwänden der Hele/Shaw-Zelle wird theoretisch und experimentell untersucht. Als Randbedingungen werden konstante Temperatur und konstante Wärmestromdichte an der Wand aufgeprägt. Das Temperaturprofil in der thermischen Grenzschicht der beheizten Wand wird mit Hilfe eines verschiebbaren Thermoelements gemessen. Mit Hilfe eines optomechanischen IR-Darstellungssystems werden Thermogramme der Strömung in der Zelle ermittelt. Die Ergebnisse aus theoretischen und experimentellen Untersuchungen stimmen gut überein. Das theoretische Modell für den Wärmeübergang durch natürliche Konvektion in einer Hele/Shaw-Zelle zeigt vollständige Übereinstimmung mit dem Modell für Wärmeübertragung durch natürliche Konvektion in einem porösen Medium, wobei der Ausdruck $h^2/12$ die Rolle der Permeabilität der Zelle spielt.

ЕСТЕСТВЕНАЯ КОНВЕКЦИЯ В УЗКОЙ ЩЕЛИ

Аннотация—Представлен теоретический и экспериментальный анализ теплообмена в условиях естественной конвекции в ячейке Хил–Шоу на узких торцевых стенках. Исследованы граничные условия первого и второго рода. Профили температур в тепловом пограничном слое на нагреваемой торцевой стенке измерялись сканирующей термопарой. Термограммы течения в ячейке получены с помощью оптико-механической тепловизионной системы. Результаты теоретического и экспериментального исследований находятся в хорошем соответствии. Показано, что теоретическая модель теплообмена при естественной конвекции в ячейке Хил–Шоу полностью соответствует модели теплообмена естественной конвекцией в пористой среде, причем роль проницаемости в ячейке Хил–Шоу играет величина $h^2/12$.